Calculation of Overtone O−H Stretching Bands and Intensities of the Water Trimer

Teemu Salmi,[†] Henrik G. Kjaergaard,[‡] and Lauri Halonen*,[†]

Laboratory of Physical Chemistry, P.O. Box 55 (A.I. Virtasen aukio 1), FIN-00014 University of Helsinki, Finland, and Department of Chemistry, University of Otago, P.O. Box 56, 9054 Dunedin, New Zealand

Received: April 3, 2009; Revised Manuscript Received: May 29, 2009

The high-frequency O−H stretching vibrational overtone spectrum of the water trimer has been studied computationally. The water trimer has been approximated as three individually vibrating water monomers. An internal coordinate Hamiltonian is constructed for each triatomic monomer unit using an exact kinetic-energy operator within the Born−Oppenheimer approximation and the two O−H distances and the H−O−H bending angle as the internal coordinates. The potential-energy surface, PES, is calculated using the coupled cluster method with single, double, and perturbative triple excitations, CCSD(T), and augmented correlation-consistent polarized valence triple-ζ, aug-cc-pVTZ, basis set. The PES is improved applying the counterpoise correction. The finite differences method is used to obtain the dipole moment surface. Eigenvalues of the Hamiltonians are computed with the variational method. Finally, matrix isolation infrared data are used to optimize some PES parameters to improve the results.

1. Introduction

The ground electronic state structures and energetics of water clusters $(H_2O)_n$, $n = 2, 3, ...$, have been of interest for some time, but it is really by a combination of modern experimental spectroscopic work and high-level electronic structure calculations that advances have been made to understand these species better.[1] In particular, the structures of the smallest water clusters, dimers and trimers, are well established. In fact, the smallest cluster, the water dimer, can even be considered to provide a good test case for advanced quantum chemistry methods. The effects of intermolecular large amplitude motions, low-frequency modes, add an additional interesting element in comparing the merits of different theoretical approaches.

The spectroscopic techniques used to study water clusters include the matrix isolation method with different hosts,[2−11] helium droplet experiments,[12−14] and gas-phase methods such as far-infrared laser absorption, infrared cavity ring-down and laser difference frequency spectroscopy in supersonic expansions, and infrared molecular beam depletion and fragment spectroscopy.[15−20] The gas-phase work has been valuable in giving information on the structures and fundamental vibrations of the smallest clusters. On the other hand, the matrix isolation studies have provided almost all experimental information on the larger clusters and on the overtone and combination states of high-frequency vibrations.

Much of the previous computational and theoretical work has concentrated on the structures and low-frequency intermolecular motions of small water clusters.[21−33] Larger systems and highly vibrationally excited states have been studied less.[34−38] The coupled cluster electronic structure calculation theory including single, double, and perturbative triple excitations [CCSD(T)] with augmented correlation-consistent valence basis sets provides the most advanced theory to study the intramolecular motions in small clusters.

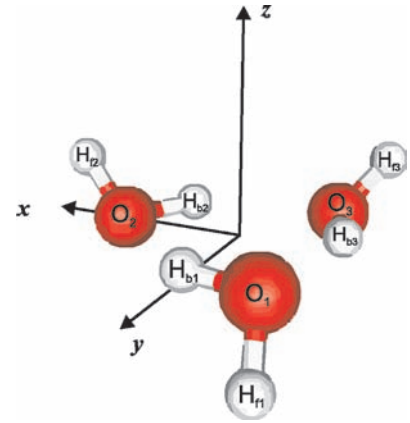

Figure 1. Global minimum energy geometry of the water trimer. The *z* axis is perpendicular to the plane containing the oxygen atoms. O_2 lies on the *x* axis.

In this work, we concentrate on the computational aspects of various isotopic species of the water trimer (WT), which in addition to the basic scientific interest might also play a role in atmospheric chemistry, although the trimer concentration is expected to be lower than that of the water monomer (WM) or dimer (WD). It has been established already some time ago that the trimer structure is cyclic. Using the notation of Schütz et al.,[26] a so-called *uud* structure, where two monomer units are pointing up (*uu*) and the other one down (*d*) from the plane containing the oxygen atoms,[3] corresponds to the minimum energy geometry. The structure is presented in Figure 1. Experimental work shows that all monomer units are equivalent.[3] Tunneling and torsional motion occur between equivalent minimum energy structures *uud*, *udu*, *duu*, *udd dud*, and *ddu*. The potential-energy barrier of both motions is close to or below the zero-point energy of WT, so the interconversion takes place rapidly between the different structures. Hence, the three monomer units are indistinguishable. We ignore the intermolecular motion in this study and assume that WT is frozen at the minimum energy geometry.

* To whom correspondence should be addressed. E-mail: lauri.halonen@helsinki.fi.
[†] University of Helsinki.
[‡] University of Otago.

10.1021/jp903088a CCC: $40.75
Published on Web 07/21/2009

We computed the structure of WT using the CCSD(T) method with the augmented correlation-consistent valence triple-ζ basis set (aug-cc-pVTZ also abbreviated as AVTZ). However, the main emphasis of this work is on the vibrational and related electronic structure calculations on potential and dipole moment surfaces. There are altogether 21 vibrational degrees of freedom in WT. Thus, at the moment, it is not feasible to include all of these in full variational calculations with an aim to obtain converged eigenvalues for highly excited vibrational states. We adopted a similar approach compared to our earlier water dimer contribution, where we included only the water monomer internal degrees of freedom in the curvilinear bond length/bond angle coordinates.[37] In practice, each monomer unit in the water trimer has been treated separately with the potential-energy surface (PES) computed for the interacting monomer units. We used within the Born−Oppenheimer approximation exact expressions of the kinetic-energy operators for each three-dimensional problem. Comparison of the water molecule results obtained using our model at the CCSD(T)/AVTZ level of theory to gas-phase observation is presented in Table 5 of ref 37.

2. Computational Details

The minimum energy structure of the water trimer as well as the potential-energy and dipole moment grids have been calculated with the Molpro program package.[39] Full 21-dimensional geometry optimization has been carried out using the CCSD(T) method with aug-cc-pVDZ (AVDZ) and aug-cc-pVTZ (AVTZ) basis sets.[40,41] The frozen core approximation was used for the 1s electrons of the oxygen atoms in all electronic structure calculations.

The effect of the basis set superposition error (BSSE) should be taken into account[42] when dealing with complexes which contain weak bonds. We used the counterpoise (CP) correction to eliminate BSSE. There is no unique way to calculate the CP correction for a three-body system. For the water trimer, we use an expression which also takes the two-body effects into account[43] in calculating the CP-corrected energy, $E^{(CP)}$, of the system, i.e.

$$\begin{aligned} E^{(CP)} &= E_{ABC}^{(ABC)} \\ &+ E_{A}^{(A)} - E_{A}^{(AB)} - E_{A}^{(AC)} + E_{A}^{(ABC)} \\ &+ E_{B}^{(B)} - E_{B}^{(AB)} - E_{B}^{(BC)} + E_{B}^{(ABC)} \\ &+ E_{C}^{(C)} - E_{C}^{(AC)} - E_{C}^{(BC)} + E_{C}^{(ABC)} \\ &+ E_{AB}^{(AB)} - E_{AB}^{(ABC)} \\ &+ E_{AC}^{(AC)} - E_{AC}^{(ABC)} \\ &+ E_{BC}^{(BC)} - E_{BC}^{(ABC)} \end{aligned} \quad (1)$$

where the labels A, B and C refer to the monomer units, the subscripts refer to the system, and the superscripts refer to the basis functions used.

One-dimensional potential-energy grids are computed performing a single-point calculation at 15 geometries for the O−H stretches and 12 for the H−O−H bends that are obtained by displacing one vibrational coordinate from the value in the optimized structure. The O−H stretching grid points are determined by changing the length of the O−H bond vector around the equilibrium value, i.e., from $r_e - 0.25$ Å to $r_e + 0.50$ Å with a step size of 0.05 Å. The bending coordinate is determined as the change in the H−O−H angle, θ, while the angle bisecting vector and the monomeric plane are kept fixed. The bending grid is calculated between −30° and +30° around the optimized geometry with steps of 5°. The two-dimensional potential-energy grids are obtained by displacing two coordinates simultaneously. We ran some test calculations for the water dimer to show that the two-dimensional part of the surface can be represented using 16 points with only a small difference in the results compared with surfaces obtained with a larger set of points. Thus, in order to keep the computational time such that the calculations are possible with the current computer resources, we used 16 points with the AVTZ basis set at $\Delta r = \pm 0.05$ and ± 0.15 Å and $\Delta\theta = \pm 5°$ and $\pm 15°$.

In order to be able to use the calculated potential-energy grid in the variational calculations, we fitted it to an analytical function using the least-squares method. As the O−H stretching coordinate we use the Morse variable $y = 1 - \exp[-a(r - r_e)]$, where a is the Morse steepness parameter and r is the instantaneous and r_e the equilibrium bond length.[44] The stretching part of the potential-energy surface possesses realistic asymptotic limits at large displacements. In practice, the stretching potential-energy function is expressed as a series expansion, i.e.

$$V(y) = \sum_i T_i y^i \qquad i = 2, 3, 4, 6 \quad (2)$$

where the T_2 parameter is called the Morse dissociation energy. We found the best possible set of i values by trying different combinations. Our previous work on the water dimer[37] helped in this respect. As the bending potential-energy function we used a series expansion over the change of the H−O−H bending angle from the equilibrium configuration, i.e.

$$V(\Delta\theta) = \sum_{i=2}^{4} \frac{f_i}{i!} (\Delta\theta)^i \quad (3)$$

where $\Delta\theta = \theta - \theta_e$. The two-dimensional part of the PES is a series expansion over bond angle displacements, $\Delta\theta$, and Morse variables, y. We obtained good results using similar potential-energy functions in our previous work.[37] One-dimensional CP-corrected potential-energy grids are calculated as the corresponding non-CP-corrected ones earlier.

We solved the internal coordinate Schrödinger equation for each monomer unit using the variational method. We employed kinetic-energy operators which are exact within the Born−Oppenheimer approximation.[45,46] The potential-energy parts are obtained as described above. Morse oscillator eigenfunctions[44] consistent with the Morse steepness parameter a and the Morse dissociation energy T_2 have been used as bases for the O−H stretching degrees of freedom, and the harmonic oscillator eigenfunctions[47] have been used for the monomer internal bending degrees of freedom. We employ the 10 first ($0 \le n \le 9$, where n is the total stretching quantum number) Morse oscillator eigenfunctions per stretch and the 10 first ($0 \le v \le 9$, where v is the bending quantum number) harmonic oscillator eigenfunctions as the bending basis. The integrals needed for Hamiltonian matrix elements are calculated as in ref 37. Test calculations show that all reported eigenvalues are converged better than 1 cm^{-1}.

The absorption intensities are calculated with a model where each monomer unit is treated separately. They are defined as the oscillator strengths of the transitions from the ground vibrational state, g, to the vibrationally excited state, e,[48] i.e.

$$f_{eg} = 4.70 \times 10^{-7}[\text{cm D}^{-2}]\tilde{\nu}_{eg}|\vec{\mu}_{eg}|^2 \quad (4)$$

where $\tilde{\nu}_{eg}$ is the transition wavenumber in cm^{-1} and $\vec{\mu}_{eg} = \langle e|\vec{\mu}|g\rangle$ is the transition dipole moment in Debye (1 D = 3.33564 × 10^{-30} Cm). The ground and upper state wave functions in the transition dipole moment integrals are obtained from the vibrational eigenvalue variational calculation of each monomer unit. The dipole moment surfaces of the three monomeric units have been computed using the CCSD(T)/AVDZ level of theory. The finite differences method has been adopted using the method described in ref 49 with electric fields of −0.0001 and +0.0001 au. The aug-cc-pVDZ basis set is small, but due to computational resources available we are unable to use the more appropriate aug-cc-pVTZ basis set in the finite difference calculations. It has previously been found that calculated oscillator strengths of O−H stretching overtone transitions using the AVDZ and AVTZ dipole moment functions differ by less than 10%.[50] This variation might be larger for the bonded O−H stretching transitions where cancellation occurs for the first and second overtone.[51] Each molecule-fixed axis component of the dipole moment function is expressed as a polynomial expansion over the bond length and bond angle displacement coordinates. The polynomial coefficients have been determined by the linear least-squares method. The one-dimensional dipole moment grid is calculated between Δr(O−H) = −0.20 Å and +0.20 Å and $\Delta\angle$(H−O−H) = −20° and +20°. The two-dimensional displacements are the same as with the PES. The molecule fixed axes used are shown in Figure 1. We did not employ Eckart axes in order to minimize vibration−rotation interactions because this alternative choice makes only a small difference.[52−54] The dipole moment surface is given in the Supporting Information.

3. Results

3.1. Geometry. The optimized geometries of WT are shown in Table 1. The results agree well with previous calculations.[29,30] The calculated hydrogen-bond angles are also similar with experimental values,[19] except that our calculated O−O distances are smaller. In the experiment, the hydrogen-bonded hydrogen atoms were assumed to lay on the oxygen plane, which according to our calculations is almost true only for H_{b1} and H_{b3} (see Table 1).

The cyclic geometry of WT possesses C_1 symmetry. The vibrational spectra of all three monomer units are unique. However, closer inspection of the structure shows similarity between monomer units 1 and 3. This can be appreciated by describing WT as three water dimers: (M1 and M2), (M2 and M3), and (M3 and M1). In the dimers (M1 and M2) and (M3 and M1), the two free hydrogen atoms are on different sides of the oxygen plane (Figure 1), so the H_f-H_f repulsion is minimized as in the water dimer. We call this configuration *parallel* and the other one in Figure 1, in which the hydrogen atoms are on the same side of the plane, *perpendicular*. The *parallel* configuration is energetically more favorable than the *perpendicular* one because of the lower H_f-H_f repulsion. Hence, the angles $\angle(O_1-H_{b1}-O_2)$ and $\angle(O_3-H_{b3}-O_1)$ associated with the hydrogen bonding are slightly larger, i.e., closer to the ideal value of 180° than to the value of $\angle(O_2-H_{b2}-O_3)$ (see Table 1). Another feature is the location of the bonded hydrogen atoms. The H_{b1} and H_{b3} atoms lie almost in the oxygen plane. The dihedral angles are 180.42° and 181.31°, respectively. On the contrary, H_{b2} is well above the plane with the dihedral angle being 166.83°. Moreover, the O_2-H_{b2} bond length is shorter than the other two $O-H_b$ bonds. On the basis of these geometrical arguments, we conclude that the $O_2-H_{b2}-O_3$ system possesses less hydrogen-bonding character than the other two $O-H_b-O$ systems in WT. Therefore, we expect a smaller red shift in the vibrational wavenumber for the $|0\rangle_f|1\rangle_b|0\rangle$ band. We used the local mode notation[35] where the subscripts f and b refer to the free and bonded hydrogen stretches, respectively, and the label without the subscripts refers to the H−O−H bend. We also expect the bonded O−H stretching vibrational spectra of the monomer units 1 and 3 to be similar. The PES parameters were obtained as described earlier and are presented in Table 2.

3.2. Energy Level Calculation. The variationally calculated energy levels of WT are presented in Table 3. We notice that the CCSD(T) method with the AVTZ basis gives good results for the free O−H stretches and the H−O−H bending modes when compared with cavity ring-down laser-spectroscopic results from ref 15. The hydrogen-bonded O−H stretching fundamental mode $|0\rangle_f|1\rangle_b|0\rangle$ is calculated to be approximately 90 cm^{-1} lower than the observation in ref 15. The corresponding difference with WD[37] is about 60 cm^{-1}. In WD, our interpretation is such that the exclusion of the intermolecular modes causes this discrepancy in our model. In WT, these differences are even more severe due to the larger number of low-frequency modes. We also ignore the coupling between the O−H stretching oscillators of the different monomer units. However, we are able to obtain a better agreement with experiment by optimizing the harmonic force constants with the nonlinear least-squares method using experimental vibrational term values from a matrix isolation study in refs 2 and 4 as data.

The CP correction improves the description of the hydrogen-bonded O−H stretch significantly but has little effect on the other vibrational modes. We made a similar observation earlier with WD, but in WT we wanted to be sure that the free hydrogen atoms do not experience a too large amount of BSSE. We performed a CP-corrected geometry optimization by searching the minimum for $E^{(CP)}$ in eq 1 with respect to the water trimer geometry parameters. On the basis of our earlier work[37] and test calculations performed for WT at the CCSD(T)/AVDZ level of theory, we assume that the CP correction has little effect on monomer geometries and intermolecular angles. Therefore, we optimize only the O−O distances with the other coordinates being fixed to the AVTZ geometry in order to keep the cost of the calculations reasonable. However, this does not describe the problem fully because when we change, for instance, the O_2-O_3 distance, one (or both) of the angles $\angle(H_{b1}-O_1-O_2)$ or $\angle(H_{b1}-O_1-O_3)$ change. The indices refer to the labels in Figure 1. Hence, we fixed all the angles of a given monomer unit to the corresponding acceptor oxygen, i.e., we fixed the intermolecular angles $\angle(H_{b1}-O_1-O_2)$, $\angle(H_{f1}-O_1-O_2)$, $\angle(H_{b2}-O_2-O_3)$, $\angle(H_{f2}-O_2-O_3)$, $\angle(H_{b3}-O_3-O_1)$, and $\angle(H_{f3}-O_3-O_1)$ as well as the dihedral angles $\tau(H_{b1}-O_1-O_2-O_3)$, $\tau(H_{f1}-O_1-O_2-O_3)$, $\tau(H_{b2}-O_2-O_3-O_1)$, $\tau(H_{f2}-O_2-O_3-O_1)$, $\tau(H_{b3}-O_3-O_1-O_2)$, and $\tau(H_{f3}-O_3-O_1-O_2)$ to the corresponding AVTZ values. The CP correction increases all the O−O distances. Since the CP correction changes the potential-energy surface, we need to calculate the energy minimum in order to be able to use our potential-energy function in variational vibrational calculations. This has been done by inserting a first-order term ($T_1 y$ for stretches and $f_\theta \Delta\theta$ for bends) into the potential-energy function in eqs 2 and 3, respectively, and finding a geometry that diminishes the coefficient of the first-order terms. The changes are minor in the case of all the coordinates.

TABLE 1: Calculated[a] Geometries of the Water Trimer

	AVDZ	AVTZ	AVTZ+CP	AVTZ+CP[b]	experiment[c]
$R(O_1-O_2)$/Å	2.8166	2.7975	2.8182[d]		2.97
$R(O_2-O_3)$/Å	2.8200	2.8044	2.8247[d]		2.94
$R(O_3-O_1)$/Å	2.8175	2.7993	2.8202[d]		2.97
r_{f1}/Å	0.9658	0.9612	0.9612	0.9610	
r_{f2}/Å	0.9654	0.9609	0.9609	0.9608	
r_{f3}/Å	0.9654	0.9609	0.9609	0.9607	
r_{b1}/Å	0.9774	0.9733	0.9733	0.9729	
r_{b2}/Å	0.9770	0.9728	0.9728	0.9724	
r_{b3}/Å	0.9776	0.9734	0.9734	0.9730	
$R(O_1-H_{b3})$/Å	1.9199	1.9051	1.9258		
$R(O_2-H_{b1})$/Å	1.9202	1.9043	1.9247		
$R(O_3-H_{b2})$/Å	1.9394	1.9260	1.9461		
θ_1/deg	104.96	105.27	105.27	105.10	
θ_2/deg	105.24	105.52	105.52	105.33	
θ_3/deg	105.18	105.43	105.43	105.26	
$\angle(O_1-H_{b1}-O_2)$/deg	151.25	151.34	151.44		152
$\angle(O_2-H_{b2}-O_3)$/deg	148.67	148.90	149.01		150
$\angle(O_3-H_{b3}-O_1)$/deg	151.42	151.48	151.58		153
$T(H_{f1}-O_1-O_2-O_3)$/deg	242.53	241.87	241.87		
$T(H_{f2}-O_2-O_3-O_1)$/deg	121.54	121.12	121.12		
$T(H_{f3}-O_3-O_1-O_2)$/deg	127.41	127.25	127.25		
$T(H_{b1}-O_1-O_2-O_3)$/deg	181.35	180.42	180.42		180
$T(H_{b2}-O_2-O_3-O_1)$/deg	165.21	166.83	166.83		180
$T(H_{b3}-O_3-O_1-O_2)$/deg	179.42	181.31	181.31		180

[a] Calculated at the CCSD(T) level of theory. [b] Calculated as the minimum of the one-dimensional PES. [c] From ref 19. [d] Optimized coordinate.

TABLE 2: Potential-Energy Surface Parameters for the Water Trimer[a]

	M1			M2			M3		
	AVTZ	AVTZ+CP	fit[b]	AVTZ	AVTZ+CP	fit[b]	AVTZ	AVTZ+CP	fit[b]
$a^{(f)}$/Å^{-1}	1.9660	1.9592	1.9592	1.9629	1.9617	1.9617	1.9665	1.9627	1.9627
$T_2^{(f)}$/aJ	1.0851	1.0931	1.0832	1.0905	1.0922	1.0788	1.0867	1.0912	1.0790
$T_3^{(f)}$/aJ	−0.1778	−0.1847		−0.1816	−0.1833		−0.1784	−0.1825	
$T_4^{(f)}$/aJ	0.0976	0.1010		0.0985	0.1008		0.0978	0.1006	
$T_6^{(f)}$/aJ	−0.0119	−0.0165		−0.0137	−0.0170		−0.0130	−0.0168	
$a^{(b)}$/Å^{-1}	2.7231	2.7028	2.7028	2.6322	2.6136	2.6136	2.7433	2.6918	2.6918
$T_2^{(b)}$/aJ	0.5033	0.5135	0.5336	0.5420	0.5525	0.5746	0.4947	0.5175	0.5402
$T_3^{(b)}$/aJ	0.0621	0.0639		0.0512	0.0524		0.0635	0.0595	
$T_4^{(b)}$/aJ	0.0454	0.0488		0.0453	0.0483		0.0448	0.0375	
$T_6^{(b)}$/aJ	−0.0112	−0.0117		−0.0118	−0.0120		−0.0108	0.0010	
$f_{r_f r_b}$/aJ Å^{-2}	−0.0762			−0.0797			−0.0785		
$f_{r_f r_b r_b}$/aJ Å^{-3}	0.1073			0.0986			0.1083		
$f_{r_f r_f r_b}$/aJ Å^{-3}	−0.1085			−0.0928			−0.1059		
$f_{\theta\theta}$/aJ	0.7224	0.7225	0.7293	0.7262	0.7217	0.7268	0.7216	0.7219	0.7293
$f_{\theta\theta\theta}$/aJ	−0.6437	−0.6648		−0.6466	−0.6745		−0.6406	−0.6600	
$f_{\theta\theta\theta\theta}$/aJ	−0.6442	−0.6366		−0.6790	−0.4279		−0.6470	−0.6417	
$f_{r_f\theta}$/aJ Å^{-1}	0.2580			0.2563			0.2579		
$f_{r_f\theta\theta}$/aJ Å^{-1}	−0.2987			−0.2964			−0.2962		
$f_{r_f r_f\theta}$/aJ Å^{-2}	−0.0913			−0.1035			−0.0945		
$f_{r_f r_f\theta\theta}$/aJ Å^{-2}	−0.1316			−0.1303			−0.1281		
$f_{r_b\theta}$/aJ Å^{-1}	0.1395			0.1408			0.1285		
$f_{r_b\theta\theta}$/aJ Å^{-1}	−0.3073			−0.2710			−0.3118		
$f_{r_b r_b\theta}$/aJ Å^{-2}	−0.4460			−0.4392			−0.4798		
$f_{r_b r_b\theta\theta}$/aJ Å^{-2}	−0.0231			0.0346			−0.0554		

[a] All angles are expressed in radians. [b] The parameters shown are obtained from fit. The others are the same with AVTZ+CP.

3.3. PES Optimization. We optimized the diagonal harmonic force constants of the CP-corrected potential-energy surfaces with the least-squares method using vibrational term values from Ar matrix infrared studies[2,4] as data. We used a similar approach earlier for WD with good results.[37] On the basis of the ab initio results in Table 3, we assume that there is an insignificant difference in the energies of the H−O−H bending as well as the free O−H stretching states between the monomer units (4 cm^{-1} for $|0\rangle_f|0\rangle_b|1\rangle$ and 4 cm^{-1} for $|1\rangle_f|0\rangle_b|0\rangle$). The difference is also only 8 cm^{-1} for their combination state $|1\rangle_f|0\rangle_b|1\rangle$. Hence, we used the same observed vibrational term values 1620, 3695, and 5292 cm^{-1} for all the monomer units in the least-squares calculations. It is difficult to locate the position of the $|1\rangle_f|0\rangle_b|0\rangle$ band because the free O−H stretching bands of other water clusters and the asymmetric stretching fundamental band ν_3 of the water monomer are nearby. The red shift of the free O−H stretching modes is small, so therefore, the ν_3 band of WM and the free O−H stretching fundamentals of WD, WT, and larger water clusters are located near each other. In addition, the intensity of the free O−H stretching fundamental is weak

TABLE 3: Calculated (CCSD(T)) and Experimental Energy Levels (cm^{-1}) for the Water Trimer (Relative Absorption Intensities in Parentheses)

	AVTZ			AVTZ+CP			fit			experiment	
local mode	M1	M2	M3	M1	M2	M3	M1	M2	M3	matrix[a]	gas phase[b]
$\|0\rangle_f\|0\rangle_b\|1\rangle$	1611	1617	1610	1611	1615	1611	1619 (14.9)	1621 (15.0)	1620 (15.3)	1620	1609, 1638
$\|0\rangle_f\|0\rangle_b\|2\rangle$	3189	3201	3188	3189	3199	3188	3206 (1.6)	3212 (1.5)	3207 (1.5)		
$\|0\rangle_f\|1\rangle_b\|0\rangle$	3439	3454	3433	3453	3467	3445	3517 (96.1)	3532 (84.5)	3517 (100)[c]	3516, 3528	3532, 3533
$\|1\rangle_f\|0\rangle_b\|0\rangle$	3706	3710	3709	3707	3711	3710	3693 (25.7)	3692 (28.4)	3693 (26.1)	3695, 3700	3726
$\|0\rangle_f\|1\rangle_b\|1\rangle$	5027	5051	5020	5041	5062	5032	5114 (1.8)	5133 (1.8)	5114 (2.1)	5114.8, 5137	
$\|1\rangle_f\|0\rangle_b\|1\rangle$	5297	5308	5300	5299	5307	5302	5294 (2.3)	5295 (2.5)	5294 (2.4)		
$\|0\rangle_f\|1\rangle_b\|2\rangle$	6573	6604	6563	6589	6618	6577	6673 (6.5×10^{-3})	6699 (8.1×10^{-3})	6672 (8.6×10^{-3})		
$\|0\rangle_f\|2\rangle_b\|0\rangle$	6691	6727	6678	6723	6756	6704	6851 (0.14)	6891 (0.082)	6849 (0.12)		
$\|1\rangle_f\|0\rangle_b\|2\rangle$	6856	6872	6858	6858	6872	6860	6862 (0.021)	6865 (0.053)	6862 (0.022)		
$\|1\rangle_f\|1\rangle_b\|0\rangle$, $\|2\rangle_f\|0\rangle_b\|0\rangle$	7116	7132	7115	7129	7144	7127	7148 (0.57)	7149 (0.62)	7146 (0.58)		
$\|2\rangle_f\|0\rangle_b\|0\rangle$, $\|1\rangle_f\|1\rangle_b\|0\rangle$	7265	7276	7272	7270	7281	7276	7269 (0.10)	7276 (0.069)	7269 (0.088)		
$\|0\rangle_f\|2\rangle_b\|1\rangle$	8260	8308	8244	8291	8336	8270	8430 (0.018)	8475 (0.019)	8426 (0.018)		
$\|1\rangle_f\|1\rangle_b\|1\rangle$, $\|2\rangle_f\|0\rangle_b\|1\rangle$	8687	8712	8684	8701	8722	8697	8730 (0.028)	8735 (0.035)	8728 (0.029)		
$\|2\rangle_f\|0\rangle_b\|1\rangle$, $\|1\rangle_f\|1\rangle_b\|1\rangle$	8837	8854	8843	8843	8858	8848	8847 (0.029)	8857 (0.023)	8847 (0.032)		
$\|0\rangle_f\|3\rangle_b\|0\rangle$, $\|0\rangle_f\|2\rangle_b\|2\rangle$	9700	9758	9678	9751	9806	9722	9932 (7.2×10^{-4})	9989 (2.3×10^{-3})	9926 (1.1×10^{-3})		
$\|0\rangle_f\|2\rangle_b\|2\rangle$, $\|0\rangle_f\|3\rangle_b\|0\rangle$	9813	9874	9794	9848	9906	9823	10 015 (1.6×10^{-3})	10 078 (3.0×10^{-3})	10 008 (1.6×10^{-3})		
$\|1\rangle_f\|2\rangle_b\|0\rangle$	10 362	10 391	10 356	10 402	10 436	10 378	10 495 (0.011)	10 508 (0.013)	10 492 (0.011)		
$\|1\rangle_f\|2\rangle_b\|0\rangle$		10 410				10 392					
$\|3\rangle_f\|0\rangle_b\|0\rangle$	10 576	10 590	10 583	10 583	10 596	10 589	10 558 (9.8×10^{-3})	10 570 (2.3×10^{-3})	10 556 (9.2×10^{-3})		
$\|2\rangle_f\|1\rangle_b\|0\rangle$	10 731	10 753	10 736	10 745	10 766	10 748	10 771 (3.6×10^{-3})	10 784 (2.2×10^{-3})	10 772 (3.2×10^{-3})		
$\|0\rangle_f\|4\rangle_b\|0\rangle$	12 524	12 616	12 491	12 607	12 691	12 560	12 859 (2.0×10^{-4})	12 946 (6.2×10^{-4})	12 850 (2.5×10^{-4})		
$\|0\rangle_f\|4\rangle_b\|0\rangle$							12 918 (1.5×10^{-4})	13 010 (5.3×10^{-4})	12 908 (1.7×10^{-4})		
$\|1\rangle_f\|3\rangle_b\|0\rangle$	13 350	13 429	13 344	13 417	13 473	13 394	13 559 (1.4×10^{-4})	13 597 (2.1×10^{-4})	13 552 (1.3×10^{-4})		
$\|1\rangle_f\|3\rangle_b\|0\rangle$	13 371	13 525	13 363	13 500	13 563	13 478	13 632 (2.1×10^{-4})	13 648 (8.8×10^{-5})	13 628 (2.0×10^{-4})		
$\|1\rangle_f\|3\rangle_b\|0\rangle$	13 460		13 445				13 662 (3.3×10^{-4})	13 714 (2.8×10^{-4})	13 656 (3.4×10^{-4})		
$\|4\rangle_f\|0\rangle_b\|0\rangle$	13 802	13 816	13 810	13 801	13 824	13 820	13 753 (9.0×10^{-4})	13 746 (1.3×10^{-4})	13 749 (7.2×10^{-4})		
$\|4\rangle_f\|0\rangle_b\|0\rangle$				13 813							
$\|2\rangle_f\|2\rangle_b\|0\rangle$	13 897	13 935	13 897	13 926	13 961	13 920	13 993 (1.8×10^{-4})	14 014 (8.6×10^{-5})	13 990 (1.6×10^{-4})		
$\|3\rangle_f\|1\rangle_b\|0\rangle$	14 109	14 140	14 115	14 130	14 160	14 133	14 168 (4.9×10^{-5})	14 189 (1.4×10^{-5})	14 169 (3.8×10^{-5})		

[a] From ref 4 except 1620 cm^{-1} is from ref 2. [b] From refs 15, 17, and 18. [c] The oscillator strength (eq 4) of this transition is 6.06×10^{-5}.

compared to corresponding bonded one. The observed Ar matrix infrared observations range from 3695[4] to 3707[3] cm^{-1}. Perchard observed two peaks 3695 and 3700 cm^{-1}, of which the latter one is more intense.[4] However, it appears as a shoulder of the WD peak at 3708 cm^{-1}, which may distort the intensity of the WT peak. We also calculate two peaks: 3707 (M1) and 3710−3711 cm^{-1} (M2 and M3), of which the intensity of the latter one is twice that of the first one. We obtain a better fit using the value 3695 cm^{-1} for all the monomer units. Using the same observation, $|1\rangle_f|0\rangle_b|1\rangle$ at 5292 cm^{-1}, for all monomer units is in line with the observation that there is just one observed vibrational band center. In the case of the bonded O−H stretch, we assign the high-intensity peaks 3516 and 5114.8 cm^{-1} to the M1 and M3 and the shoulder values 3528 and 5137 cm^{-1} to M2. In the O−H stretching overtone region, $|0\rangle_f|2\rangle_b|0\rangle$ is below 6800 cm^{-1} according to ref 4. The other two stretching vibrational overtone states are at 7188.5 and 7201 cm^{-1}. We are unable to include these in the fit. Instead, we calculated these two states, which consist of $|2\rangle_f|0\rangle_b|0\rangle$ and $|1\rangle_f|1\rangle_b|0\rangle$, to be at 7146−7149 and 7269−7276 cm^{-1}. The states are heavily mixed. Looking at Figure 7 in ref 4 we find two peaks located at ∼7150 and ∼7270 cm^{-1}, both of which increase as the Ar/H_2O ratio is lowered. However, according to our calculations, the intensity of the first one is about seven times the intensity of the latter one, while the intensities are equal in Figure 7 of ref 4. WD bands have been calculated to be at 7199, 7238, and 7249 cm^{-1}.[37] The observed band at 7270 cm^{-1} appears as a shoulder of a higher peak. Therefore, it could be that its true intensity is lower than in Figure 7 of ref 4. Anyway, we suggest these assignments to the observed matrix spectrum.

3.4. O−H Stretching Overtones. In the first O−H stretching vibrational overtone region, the state $|0\rangle_f|2\rangle_b|0\rangle$ is well separated from the other stretching states $|1\rangle_f|1\rangle_b|0\rangle$ and $|2\rangle_f|0\rangle_b|0\rangle$, which are mixed. At the CCSD(T)/AVTZ level of theory, the mixing ratio is approximately 75−20%. Applying the CP correction to the one-dimensional PES slices increases the mixing slightly. Optimizing the harmonic force constants raises the hydrogen-bonded O−H stretching energy levels, so that the mixing ratio becomes roughly 50−50%. A similar behavior is observed in the two quanta of stretching and one quantum of bending overtone region. After optimizing the harmonic force constants, the energy of $|0\rangle_f|2\rangle_b|0\rangle$ rises close to $|1\rangle_f|0\rangle_b|2\rangle$, causing an anharmonic resonance between these two states. These states are directly coupled by the kinetic-energy terms of our model. The appropriate higher order potential-energy coupling terms are absent in our treatment. We would rather expect a cubic anharmonic resonance, Fermi resonance,[55] to occur between $|0\rangle_f|2\rangle_b|0\rangle$ and $|0\rangle_f|1\rangle_b|2\rangle$. However, the states are not mixed;, for instance, in M1, the state at 6673 cm^{-1} is 82% of $|0\rangle_f|1\rangle_b|2\rangle$ and only 4% of $|0\rangle_f|2\rangle_b|0\rangle$ whereas the one at 6851 cm^{-1} is 78% of $|0\rangle_f|2\rangle_b|0\rangle$, 17% of $|1\rangle_f|0\rangle_b|2\rangle$, and 1% of $|0\rangle_f|1\rangle_b|2\rangle$. This kind of behavior is also observed in M3. In M2, the $|0\rangle_f|2\rangle_b|0\rangle$ state is well separated from $|1\rangle_f|0\rangle_b|2\rangle$, and consequently, coupling is not observed.

In the second overtone region we observe a Fermi resonance between $|0\rangle_f|3\rangle_b|0\rangle$ and $|0\rangle_f|2\rangle_b|2\rangle$. The mixing ratio is 80−15% at the CCSD(T)/AVTZ level of theory. Applying the CP correction increases the energies of the bonded O−H stretching states and therefore also increases the mixing to 75−20%. However, as we noted in Table 3, even after the CP correction the bonded O−H stretching fundamental is ∼80 cm^{-1} lower than the observation. This resonance is sensitive to small changes in PES, so optimizing the harmonic force constants with the Ar matrix observations as data changes the picture. The upper state gains more $|0\rangle_f|3\rangle_b|0\rangle$ character, and the mixing ratio becomes 50−50%. The absorption intensity of the transition from the ground vibrational state to the upper state also exceeds the intensity of the transition to the lower state. The

TABLE 4: Comparison of Calculated and Experimental Fundamental Term Values (cm^{-1})

local mode	this work	Wang et al.[a]	gas phase	He droplet	Ar matrix[b]	Ar matrix[c]
			$(H_2O)_3$			
$\|0\rangle_f\|0\rangle_b\|1\rangle$	1611, 1611, 1615	1646, 1659, 1674	1609, 1638[d]		1602, 1620, 1632	1602
$\|0\rangle_f\|1\rangle_b\|0\rangle$	3445, 3453, 3467	3463, 3533, 3544	3532;[d] 3533[e]	3529, 3544[g]	3516, 3528	3516, 3527
$\|1\rangle_f\|0\rangle_b\|0\rangle$	3707, 3710, 3711	3750, 3754, 3765	3726[e]		3695, 3700	3707
			$(D_2O)_3$			
$\|0\rangle_f\|0\rangle_b\|1\rangle$	1189, 1189, 1192	1218, 1229, 1234			1183, 1196	1183
$\|0\rangle_f\|1\rangle_b\|0\rangle$	2539, 2543, 2552	2563, 2602, 2609	2588, 2592[f]		2580, 2592	2579
$\|1\rangle_f\|0\rangle_b\|0\rangle$	2739, 2741, 2743	2772, 2774, 2781	2756[f]		2733, 2738	2738

[a] From ref 29. [b] From refs 2 and 7. [c] From ref 3. [d] From ref 17. [e] From ref 18. [f] From ref 16. [g] From ref 13.

other three O−H stretching modes, denoted in Table 3 as $|1\rangle_f|2\rangle_b|0\rangle$, $|3\rangle_f|0\rangle_b|0\rangle$, and $|2\rangle_f|1\rangle_b|0\rangle$, are combinations of these three states. The states in Table 3 have been assigned using the quantum numbers of the basis function with the largest contribution to the eigenstate. At the AVTZ level of theory, in energy the lowest of these three states is well separated from the other two states and is coupled with $|2\rangle_f|0\rangle_b|2\rangle$. The state is almost purely $|1\rangle_f|2\rangle_b|0\rangle$ at the AVTZ+CP level of theory. Again, the fit raises the bonded O−H stretching levels so that $|1\rangle_f|2\rangle_b|0\rangle$ mixes with $|3\rangle_f|0\rangle_b|0\rangle$ and $|2\rangle_f|1\rangle_b|0\rangle$.

In the third overtone region, the $|0\rangle_f|4\rangle_b|0\rangle$ states are well separated from the others. The red shift from the nearest WM level, $|40\rangle^+|0\rangle$ (for the local mode notation of this symmetric case see refs 56 and 57) is more than 1000 cm^{-1} at the AVTZ+CP level of theory. As found earlier, the level from the least-squares calculation is higher in energy than the pure ab initio value. In the cases of all the monomer units, the fitted $|0\rangle_f|4\rangle_b|0\rangle$ region consists of two states, which are combinations of $|0\rangle_f|4\rangle_b|0\rangle$, $|0\rangle_f|3\rangle_b|2\rangle$, and states with higher bending character. The $|1\rangle_f|3\rangle_b|0\rangle$ states consist of two or three energy levels which are combinations of $|1\rangle_f|3\rangle_b|0\rangle$ and states with more pronounced bending character. The other two energy levels of the third overtone region are combinations of $|4\rangle_f|0\rangle_b|0\rangle$, $|3\rangle_f|1\rangle_b|0\rangle$, and $|2\rangle_f|2\rangle_b|0\rangle$.

3.5. Intensity Calculation. The infrared one-photon absorption intensities of transitions from the ground vibrational state are calculated using eq 4 and scaled so that the value of 100 is attached to the most intense transition which is from the ground state to the hydrogen-bonded O−H stretching $|0\rangle_f|1\rangle_b|0\rangle$ of the monomer unit 3. The calculated intensities are presented in Table 3. The intensity of the strongest band is 3.5 times the intensity of the second strongest band $|1\rangle_f|0\rangle_b|0\rangle$. However, the $|1\rangle_f|0\rangle_b|0\rangle$ states are within 1 cm^{-1}, whereas that of the $|0\rangle_f|1\rangle_b|0\rangle$ states is 15 cm^{-1} from the other two. This enhances the $|1\rangle_f|0\rangle_b|0\rangle$ peak because the intensity maxima are close to each other. The order is reversed in the overtone region in the sense that the intensity of the hydrogen-bonded O−H stretching band is not the largest one. This agrees with the observations[4,5] where the $|0\rangle_f|2\rangle_b|0\rangle$ band is too weak to be detected. This is also in agreement with the experiment[20] and calculations[34−38] for WD.

3.6. Comparison to Other Computational Works. We compare our calculated results with a recently published study by Wang et al.[29] They computed the intramolecular fundamentals using the MULTIMODE program with a PES calculated at the ACPF/cc-pVTZ level of theory. A comparison of our calculated results to the ones in ref 29 is presented in Table 4. There is a difference between the same mode of different monomer units. Our calculated bending modes are within 4 cm^{-1} of each other, while the difference is 28 cm^{-1} in ref 29. An IR-CRLAS experiment[17] shows two WT bending bands: one located at 1609 and the other at 1638 cm^{-1}. An Ar matrix infrared spectroscopic experiment gives bands at 1602, 1620, and 1632 cm^{-1}. Our calculated spectrum shows two peaks centered at 1611 and 1615 cm^{-1}. However, the observed spectra contain close-lying bending fundamentals of many sizes of water clusters. The separation of the band centers belonging to the three monomer units in ref 29 is even larger in bonded O−H stretching vibrations: 81 cm^{-1}. The band in the middle is located at the same wavenumber as the gas-phase observation.[18] We simulated the spectrum of WT using the Lorentzian band shape with a fwhm (full width at half-maximum) of 15 cm^{-1} and plotted the spectrum in the fundamental O−H stretching region in Figure 2. Our calculated hydrogen-bonded O−H stretching spectrum possesses a shape that is similar to the experimental ones[11,15] where the high peak contains a shoulder at the high wavenumber side. The higher peak is due to the *perpendicular* M1 and M3. The shoulder originates from the *parallel* M2, the upper state of which is about 15 cm^{-1} higher in energy. Thus, although our calculated energies are too low, we qualitatively obtain the right picture, i.e., our spectrum is similar to the observed one. All of our calculated free O−H stretching fundamentals are close to those in refs 2, 3, 12, and 18.

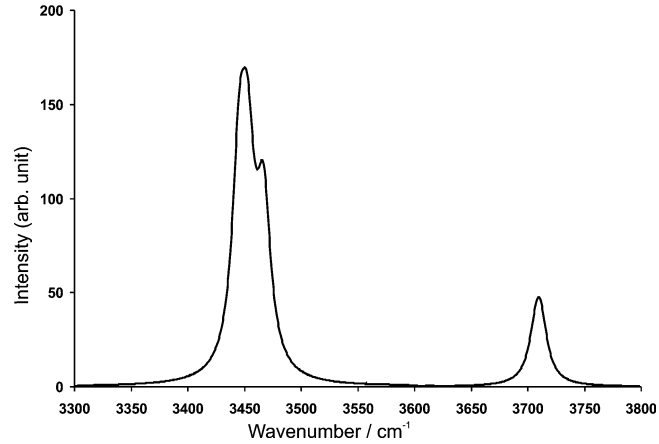

Figure 2. Simulated (CCSD(T)/AVTZ+CP) water trimer O−H stretching vibrational absorption spectrum, fwhm = 15 cm^{-1}.

For WD it was found, within a harmonically coupled anharmonic oscillator model (HCAO) approach, that coupling between the O−H stretching modes of different water units is small.[38] The effect of including this coupling changed frequencies by less than 5 cm^{-1} in the fundamental and first overtone region. Not surprisingly, absorption intensities were found to be more sensitive to this coupling, which mixes states with significantly different intensities. The intensities were found to change as much as 50% upon inclusion of the coupling.[38] For WD, it was also found that coupling to the lower frequency intermolecular modes increases the frequency of the O−H stretching modes[38] similar to the differences seen in Table 4 between the current calculation and the vibrational configuration interaction calculation of ref 29.

TABLE 5: Calculated (CCSD(T)/AVTZ+CP) and Experimental Energy Levels (cm^{-1}) and Relative Absorption Intensities (CCSD(T)/AVDZ) for the Deuterated Water Trimer $(D_2O)_3$ (Intensities in Parentheses)

local mode	M1	M2	M3	Ar matrix[a]
$\|0\rangle_f\|0\rangle_b\|1\rangle$	1189 (15.5)	1192 (15.6)	1189 (16.0)	1183 (m), 1196 (m)
$\|0\rangle_f\|0\rangle_b\|2\rangle$	2360 (2.2)	2366 (2.2)	2360 (2.2)	
$\|0\rangle_f\|1\rangle_b\|0\rangle$	2543 (95.5)	2552 (85.6)	2539 (100)[b]	2580 (s)
$\|1\rangle_f\|0\rangle_b\|0\rangle$	2739 (30.1)	2743 (30.8)	2741 (29.4)	2733 (m), 2738 (m)
$\|0\rangle_f\|1\rangle_b\|1\rangle$	3723 (1.3)	3736 (1.3)	3718 (1.5)	
$\|1\rangle_f\|0\rangle_b\|1\rangle$	3918 (2.0)	3925 (2.1)	3921 (2.1)	
$\|0\rangle_f\|2\rangle_b\|0\rangle$	4999 (0.12)	5019 (0.11)	4988 (0.11)	
$\|1\rangle_f\|1\rangle_b\|0\rangle$	5253 (0.38)	5263 (0.40)	5252 (0.37)	
$\|2\rangle_f\|0\rangle_b\|0\rangle$	5407 (0.24)	5416 (0.23)	5411 (0.25)	
$\|0\rangle_f\|2\rangle_b\|2\rangle$, $\|0\rangle_f\|3\rangle_b\|0\rangle$	7301 (6.3×10^{-4})	7333 (1.9×10^{-3})	7286 (9.4×10^{-4})[c]	
$\|0\rangle_f\|3\rangle_b\|0\rangle$, $\|0\rangle_f\|2\rangle_b\|2\rangle$	7368 (1.6×10^{-3})	7404 (3.1×10^{-3})	7347 (5.3×10^{-4})[c]	
$\|0\rangle_f\|3\rangle_b\|0\rangle$, $\|0\rangle_f\|2\rangle_b\|2\rangle$			7352 (1.1×10^{-3})[c]	
$\|1\rangle_f\|2\rangle_b\|0\rangle$	7701 (2.7×10^{-3})	7721 (2.7×10^{-3})	7694 (2.6×10^{-3})	
$\|3\rangle_f\|0\rangle_b\|0\rangle$	7863 (7.5×10^{-3})	7876 (4.8×10^{-3})	7866 (7.2×10^{-3})	
$\|2\rangle_f\|1\rangle_b\|0\rangle$	8018 (6.9×10^{-3})	8033 (4.3×10^{-3})	8022 (6.8×10^{-3})	
$\|0\rangle_f\|4\rangle_b\|0\rangle$	9578 (8.1×10^{-5})	9640 (4.8×10^{-4})	9559 (2.2×10^{-4})	
$\|0\rangle_f\|4\rangle_b\|0\rangle$	9590 (1.5×10^{-4})			
$\|1\rangle_f\|3\rangle_b\|0\rangle$	10 065 (4.9×10^{-5})	10 101 (5.9×10^{-5})	10 051 (4.4×10^{-5})	
$\|2\rangle_f\|2\rangle_b\|0\rangle$, $\|3\rangle_f\|1\rangle_b\|0\rangle$, $\|4\rangle_f\|0\rangle_b\|0\rangle$	10 284 (1.5×10^{-4})	10 301 (5.6×10^{-5})	10 285 (1.0×10^{-4})	
$\|2\rangle_f\|2\rangle_b\|0\rangle$, $\|4\rangle_f\|0\rangle_b\|0\rangle$	10 401 (4.5×10^{-4})	10 422 (1.7×10^{-4})	10 404 (4.1×10^{-4})	
$\|2\rangle_f\|2\rangle_b\|0\rangle$, $\|3\rangle_f\|1\rangle_b\|0\rangle$, $\|4\rangle_f\|0\rangle_b\|0\rangle$	10 578 (1.2×10^{-4})	10 600 (4.1×10^{-5})	10 582 (1.1×10^{-4})	

[a] From ref 7, m = medium; s = strong in intensity. [b] The oscillator strength (eq 4) of this transition is 3.06×10^{-5}. [c] States at 7286, 7347, and 7352 cm^{-1} are combinations of $|0\rangle_f|3\rangle_b|0\rangle$, $|0\rangle_f|2\rangle_b|2\rangle$, and higher-order bending states.

TABLE 6: Calculated (CCSD(T)/AVTZ + CP) and Experimental Energy Levels (cm^{-1}) and Relative Absorption Intensities (CCSD(T)/AVDZ) for the Partially Deuterated Water Trimer $(H_f-O-D_b)_3$ (Intensities in Parentheses)

local mode	M1	M2	M3	Ar matrix[a]
$\|0\rangle_f\|0\rangle_b\|1\rangle$	1420 (22.5)	1423 (22.6)	1420 (23.1)	1389 (m)
$\|0\rangle_f\|1\rangle_b\|0\rangle$	2554 (116)	2563 (107)	2550 (121)	2587 (m), 2596 (m)
$\|0\rangle_f\|0\rangle_b\|2\rangle$	2818 (0.24)	2826 (0.30)	2818 (0.26)	
$\|1\rangle_f\|0\rangle_b\|0\rangle$	3699 (17.1)	3702 (17.0)	3702 (15.7)	
$\|0\rangle_f\|1\rangle_b\|1\rangle$	3959 (3.0)	3972 (3.1)	3954 (3.4)	
$\|0\rangle_f\|2\rangle_b\|0\rangle$	5007 (0.10)	5028 (0.083)	4995 (0.094)	
$\|1\rangle_f\|0\rangle_b\|1\rangle$	5099 (2.3)	5105 (2.4)	5102 (2.3)	
$\|1\rangle_f\|1\rangle_b\|0\rangle$	6246 (0.20)	6259 (0.21)	6245 (0.21)	
$\|2\rangle_f\|0\rangle_b\|0\rangle$	7237 (1.1)	7244 (1.1)	7244 (1.1)	
$\|0\rangle_f\|3\rangle_b\|0\rangle$	7356 (2.9×10^{-3})	7390 (5.8×10^{-3})	7336 (3.3×10^{-3})	
$\|2\rangle_f\|0\rangle_b\|1\rangle$	8617 (0.10)	8628 (0.10)	8624 (0.11)	
$\|1\rangle_f\|2\rangle_b\|0\rangle$	8685 (8.9×10^{-4})	8711 (9.7×10^{-4})	8673 (1.0×10^{-3})	
$\|0\rangle_f\|4\rangle_b\|0\rangle$	9597 (3.2×10^{-4})	9649 (7.9×10^{-4})	9568 (3.4×10^{-4})	
$\|2\rangle_f\|1\rangle_b\|0\rangle$	9779 (2.5×10^{-3})	9795 (2.5×10^{-3})	9782 (2.5×10^{-3})	
$\|3\rangle_f\|0\rangle_b\|0\rangle$	10 617 (0.045)	10 627 (0.030)	10 627 (0.043)	
$\|1\rangle_f\|3\rangle_b\|0\rangle$	11 048 (7.6×10^{-5})	11 087 (8.3×10^{-5})	11 031 (6.9×10^{-5})	
$\|0\rangle_f\|5\rangle_b\|0\rangle$	11 729 (6.7×10^{-5})	11 801 (1.4×10^{-4})	11 691 (7.0×10^{-5})	
$\|2\rangle_f\|2\rangle_b\|0\rangle$	12 219 (3.8×10^{-5})	12 247 (3.0×10^{-5})	12 214 (3.9×10^{-5})	
$\|3\rangle_f\|1\rangle_b\|0\rangle$	13 153 (1.3×10^{-4})	13 172 (9.5×10^{-5})	13 159 (1.3×10^{-4})	
$\|1\rangle_f\|4\rangle_b\|0\rangle$	13 281 (4.8×10^{-6})	13 336 (8.0×10^{-5})	13 255 (3.9×10^{-6})	
$\|4\rangle_f\|0\rangle_b\|0\rangle$	13 839 (2.9×10^{-3})	13 853 (9.7×10^{-4})	13 853 (2.5×10^{-3})	

[a] From ref 7, m = medium in intensity.

We find similar features in the O−H stretching bands when comparing our results to an earlier HCAO calculation.[34] The free O−H stretching bands of all three monomer units are located close to each other. Even in the case of the third overtone band $|4\rangle_f|0\rangle_b|0\rangle$, they are only 11 cm^{-1} apart in ref 34. The bonded O−H stretching fundamentals and overtone spectra are also similar, i.e., the bands belonging to M1 and M3 are close and the M2 bands are slightly higher in wavenumber. Our calculated intensities agree with the previous result. Hence, we confirm the earlier calculations[34] in a qualitative way.

3.7. Deuterated Species. We also calculated the spectra of fully and partially deuterated WT. The results are shown in Tables 5−7. The calculations of these species have been carried out using the CCSD(T)/AVTZ+CP geometry and PES. The relative intensities are scaled so that transition from the ground state to $|0\rangle_f|1\rangle_b|0\rangle$ of fully deuterated monomer unit 3 assumes the value 100. Albeit the fitted PES is in practice mass independent, the optimized parameters may depend on the isotopic species due to some contribution from the kinetic-energy operator of the intermolecular modes of WT. Hence, the use of the fitted PES with deuterated species is questionable. The calculated spectrum of $(D_2O)_3$ closely resembles that of $(H_2O)_3$ computed at the same level of theory. In the bending fundamental region all three $|0\rangle_f|0\rangle_b|1\rangle$ levels are located close to each other at 1189, 1192, and 1189 cm^{-1}. The intensities of the transitions from the ground vibrational state to these excited states are almost equal. The band centers are close to an Ar matrix infrared spectroscopic observation[7] at 1196 cm^{-1}. The bonded O−D stretching fundamentals are at 2543, 2552, and 2539 cm^{-1} according to our results. If we assume the maximum

TABLE 7: Calculated (CCSD(T)/AVTZ + CP) Energy Levels (cm^{-1}) and Relative Absorption Intensities (CCSD(T)/AVDZ) for the Partially Deuterated Water Trimer $(D_f-O-H_b)_3$ (Intensities in Parentheses)

local mode	M1	M2	M3
$\|0\rangle_f\|0\rangle_b\|1\rangle$	1414 (22.5)	1417 (22.7)	1414 (23.2)
$\|1\rangle_f\|0\rangle_b\|0\rangle$	2718 (5.1)	2720 (4.8)	2720 (4.3)
$\|0\rangle_f\|0\rangle_b\|2\rangle$	2806 (1.8)	2815 (1.8)	2805 (1.7)
$\|0\rangle_f\|1\rangle_b\|0\rangle$	3463 (232)	3477 (214)	3456 (242)
$\|1\rangle_f\|0\rangle_b\|1\rangle$	4115 (0.95)	4121 (1.0)	4116 (0.91)
$\|0\rangle_f\|1\rangle_b\|1\rangle$	4852 (5.1)	4872 (5.3)	4843 (5.8)
$\|2\rangle_f\|0\rangle_b\|0\rangle$	5353 (0.57)	5358 (0.59)	5358 (0.58)
$\|1\rangle_f\|1\rangle_b\|0\rangle$	6171 (0.11)	6189 (0.11)	6165 (0.11)
$\|0\rangle_f\|2\rangle_b\|0\rangle$	6732 (0.29)	6765 (0.23)	6713 (0.25)
$\|3\rangle_f\|0\rangle_b\|0\rangle$	7904 (0.016)	7911 (0.011)	7912 (0.016)
$\|2\rangle_f\|1\rangle_b\|0\rangle$	8802 (1.7×10^{-3})	8821 (1.5×10^{-3})	8798 (1.6×10^{-3})
$\|0\rangle_f\|2\rangle_b\|2\rangle$, $\|1\rangle_f\|2\rangle_b\|0\rangle$	9417 (8.3×10^{-4})	9459 (1.6×10^{-3})	9396 (9.6×10^{-4})
$\|1\rangle_f\|2\rangle_b\|0\rangle$, $\|0\rangle_f\|2\rangle_b\|2\rangle$	9450 (6.7×10^{-4})	9495 (4.6×10^{-4})	9431 (8.1×10^{-4})
$\|0\rangle_f\|3\rangle_b\|0\rangle$	9802 (5.5×10^{-3})	9860 (0.012)	9772 (6.1×10^{-3})
$\|4\rangle_f\|0\rangle_b\|0\rangle$	10 372 (8.3×10^{-4})	10 381 (3.2×10^{-4})	10 381 (7.4×10^{-4})
$\|3\rangle_f\|1\rangle_b\|0\rangle$	11 349 (7.9×10^{-5})	11 370 (5.8×10^{-5})	11 348 (7.5×10^{-5})
$\|2\rangle_f\|2\rangle_b\|0\rangle$	12 054 (3.0×10^{-5})	12 098 (2.2×10^{-5})	12 038 (3.5×10^{-5})
$\|1\rangle_f\|3\rangle_b\|0\rangle$	12 495 (3.4×10^{-5})	12 563 (5.6×10^{-5})	12 463 (6.3×10^{-5})
$\|0\rangle_f\|4\rangle_b\|0\rangle$	12 682 (8.7×10^{-4})	12 768 (2.2×10^{-3})	12 644 (9.6×10^{-4})

to be located in the midpoint of M1 and M3 and the shoulder at M2, their separation is 11 cm^{-1}. This kind of shoulder has not been observed.

The results from previous Ar and Kr matrix infrared studies[3] show that replacing the hydrogen atoms of the other monomer units with deuterium ones lowers the bonded O−H stretching wavenumbers of a given monomer unit, i.e., brings them closer to our calculated states $|0\rangle_f|1\rangle_b|0\rangle$. The Kr matrix values change from 3514.2 cm^{-1} for $(H_2O)_3$ to 3497.3 cm^{-1} for $H_2O(D_2O)_2$. Our model treats the monomer units separately, which is closer to the latter case where the O−H stretches of different monomer units are more weakly coupled because of the H/D mass difference. It is pleasing to see the observations approaching our calculations when the mass of the other hydrogen atoms is increased.

4. Conclusions

We calculated the O−H stretching vibrational overtone spectrum of the water trimer using a model that describes the trimer as three individually vibrating monomer units. The potential-energy surface is affected by the presence of the other monomer units, although we include only direct couplings between internal degrees of freedom of a given monomer unit. We previously used a similar model with the water dimer and obtained a good agreement with experiments.[37] In our previous study, we calculated the spectrum of WD at the CCSD(T)/AVTZ level of theory. The calculation was also performed using complete basis set limit extrapolation, core−valence, and relativistic corrections on the one-dimensional PES slices. It is not feasible to apply these corrections to WT due to the high computational cost. However, the WD results allow us to evaluate the limits of our model. In WD, these corrections rise energies of all fundamental O−H stretches by approximately 25 cm^{-1}, which brings the free O−H stretches close to gas-phase observations.[18] The wavenumber of the bonded O−H stretching fundamental is also improved but is still 42 cm^{-1} too low. The CCSD(T)/AVTZ method is sufficient for the H−O−H bending modes because the corrections have only a small effect on them. A similar result was also obtained when the calculations were repeated for the water molecule.[37] When the calculated bonded O−H stretching fundamentals are compared with the gas-phase observations,[18] it is found that the difference between the observed and the calculated wavenumber is 90 cm^{-1} for the trimer but only 60 cm^{-1} for the dimer at the CCSD(T)/AVTZ level of theory. For the free O−H stretches, the corresponding numbers are 16 and 25 cm^{-1}, respectively. It seems that the neglect of intermolecular modes in the model causes more problems in the calculated bonded O−H stretches of WT than in WD. However, the model works better in the case of the free O−H stretches of WT than in WD. We can estimate the limits of our model using the WM and WD calculations as a reference. On the basis of these results, we would assume roughly a 25 cm^{-1} rise to the position of the $|0\rangle_f|1\rangle_b|0\rangle$ band, making the difference from the experimental result 65 cm^{-1} when the basis set size is increased from AVTZ to AVQZ and the above-mentioned corrections are applied. Hence, increasing the basis set size and improving the method would not make a large improvement. Thus, the CCSD(T)/AVTZ level of theory is sufficient for WT.

We obtain improved results for the vibrational levels of WT by optimizing some of the harmonic force constants of the ab initio PES with the least-squares method and using experimental observations as data. We are able to propose new assignments in the first O−H stretching overtone region of an experimental spectrum by using experimental data only from the O−H stretching and H−O−H bending fundamental and combination band region. This gives us confidence in the higher overtone results for which there are not yet any available experimental results. Our work should help in assigning future matrix isolation and gas-phase infrared spectra. This study together with our earlier work on WD can be used to assign spectra of larger water clusters in eliminating the absorption features of smaller clusters in congested vibrational spectra.

Acknowledgment. We thank the Academy of Finland, the University of Helsinki, the Marsden Fund administered by the Royal Society of New Zealand, and the QUASAAR EU-funded network for financial support. We also thank CSC Scientific Computing Ltd. for providing computing time. We thank Anna Garden, Joseph Lane, Nino Runeberg, and Vesa Hänninen for helpful discussions.

Supporting Information Available: Description of the dipole moment surface for the water trimer. This material is available free of charge via the Internet at http://pubs.acs.org.

References and Notes

(1) Keutsch, F. N.; Cruzan, J. D.; Saykally, R. J. *Chem. Rev.* **2003**, *103*, 2533.
(2) Bentwood, R. M.; Barnes, A. J.; Orville-Thomas, W. J. *J. Mol. Spectrosc.* **1980**, *84*, 391.
(3) Engdahl, A.; Nelander, B. *J. Chem. Phys.* **1987**, *86*, 4831.
(4) Perchard, J. P. *Chem. Phys.* **2001**, *273*, 217.
(5) Perchard, J. P. *Chem. Phys.* **2001**, *266*, 109.
(6) Engdahl, A.; Nelander, B. *J. Mol. Struct.* **1989**, *193*, 101.
(7) (a) Ayers, P. G.; Pullin, A. D. E. *Spectrochim. Acta* **1975**, *32A*, 1629. (b) Ayers, P. G.; Pullin, A. D. E. *Spectrochim. Acta* **1975**, *32A*, 1641. (c) Ayers, P. G.; Pullin, A. D. E. *Spectrochim. Acta* **1975**, *32A*, 1689. (d) Ayers, P. G.; Pullin, A. D. E. *Spectrochim. Acta* **1975**, *32A*, 1695.
(8) Ceponkus, J.; Uvdal, P.; Nelander, B. *J. Phys. Chem. A* **2008**, *112*, 3921.
(9) Ohno, K.; Okimura, M.; Akai, N.; Katsumoto, Y. *Phys. Chem. Chem. Phys.* **2005**, *7*, 3005.
(10) Hirabayashi, S.; Yamada, K. M. T. *J. Chem. Phys.* **2005**, *122*, 244501.
(11) Hirabayashi, S.; Yamada, K. M. T. *J. Mol. Struct.* **2006**, *795*, 78.
(12) Fröchtenicht, R.; Kaloudis, M.; Koch, M.; Huisken, F. *J. Chem. Phys.* **1996**, *105*, 6128.
(13) Burnham, C. J.; Xantheas, S. S.; Miller, M. A.; Applegate, B. E.; Miller, R. E. *J. Chem. Phys.* **2002**, *117*, 1109.
(14) Slipchenko, M. N.; Kuyanov, K. E.; Sartakov, B. G.; Vilesov, A. F. *J. Chem. Phys.* **2006**, *124*, 241101.
(15) Paul, J. B.; Collier, C. P.; Saykally, R. J.; Scherer, J. J.; O'Keefe, A. *J. Phys. Chem. A* **1997**, *101*, 5211.
(16) Paul, J. B.; Provencal, R. A.; Petterson, A.; Saykally, R. J. *J. Chem. Phys.* **1998**, *109*, 10201.
(17) Paul, J. B.; Provencal, R. A.; Chapo, C.; Petterson, A.; Saykally, R. J. *J. Phys. Chem. A* **1999**, *103*, 2972.
(18) Huisken, F.; Kaloudis, M.; Kulcke, A. *J. Chem. Phys.* **1996**, *104*, 17.
(19) Pugliano, N.; Saykally, R. J. *Science* **1992**, *257*, 1937.
(20) Nizkorodov, S. A.; Ziemkiewicz, M.; Nesbitt, D. J.; Knight, A. E. W. *J. Chem. Phys.* **2005**, *122*, 194316.
(21) Åstrand, P.-O.; Karlström, G.; Engdahl, A.; Nelander, B. *J. Chem. Phys.* **1995**, *102*, 3534.
(22) Anderson, J. A.; Crager, K.; Fedoroff, L.; Tschumper, G. S. *J. Chem. Phys.* **2004**, *121*, 11023.
(23) Dunn, M. E.; Evans, T. M.; Kirschner, A.; Shields, G. C. *J. Phys. Chem. A* **2006**, *110*, 303.
(24) Estrin, D. A.; Paglieri, L.; Corongiu, G.; Clementi, E. *J. Phys. Chem.* **1996**, *100*, 8701.
(25) Milet, A.; Moszynski, R.; Wormer, P. E. S.; van der Avoird, A. *J. Phys. Chem. A* **2003**, *103*, 6811.
(26) Schütz, M.; Bürgl, T.; Leutwyler, S.; Bürgl, H. B. *J. Chem. Phys.* **1993**, *99*, 5228.
(27) Taketsugu, T.; Wales, D. J. *Mol. Phys.* **2002**, *100*, 2793.
(28) van der Avoird, A.; Szalewicz, K. *J. Chem. Phys.* **2008**, *128*, 014302.
(29) Wang, Y.; Carter, S.; Braams, B. J.; Bowman, J. M. *J. Chem. Phys.* **2008**, *128*, 071101.
(30) Xantheas, S. S.; Dunning, T. H., Jr. *J. Chem. Phys.* **1993**, *98*, 8037.
(31) Xantheas, S. S.; Dunning, T. H., Jr. *J. Chem. Phys.* **1993**, *99*, 8774.
(32) Losada, M.; Leutwyler, S. *J. Chem. Phys.* **2002**, *117*, 2003.
(33) Huang, X.; Braams, B. J.; Bowman, J. M. *J. Phys. Chem. A* **2006**, *110*, 445.
(34) Low, G. R.; Kjaergaard, H. G. *J. Chem. Phys.* **1999**, *110*, 9104.
(35) Schofield, D. P.; Kjaergaard, H. G. *Phys. Chem. Chem. Phys.* **2003**, *5*, 3100.
(36) Schofield, D. P.; Lane, J. R.; Kjaergaard, H. G. *J. Phys. Chem. A* **2007**, *111*, 567.
(37) Salmi, T.; Hänninen, V.; Garden, A. E.; Kjaergaard, H. G.; Tennyson, J.; Halonen, L. *J. Phys. Chem. A* **2008**, *112*, 6305 The T_6 parameters are constrained to zero in all variational calculations.
(38) Kjaergaard, H. G.; Garden, A. L.; Chaban, G. M.; Gerber, R. B.; Matthews, D. A.; Stanton, J. F. *J. Phys. Chem. A* **2008**, *112*, 4324.
(39) Werner, H.-J.; Knowles, P. J.; Lindh, R.; Manby, F. R.; Schütz, M. et al. *MOLPRO, version 2006.1, a package of ab initio programs*; 2006, see http://www.molpro.net.
(40) Kendall, R. A.; Dunning, T. H., Jr.; Harrison, R. J. *J. Chem. Phys.* **1992**, *96*, 6796.
(41) Dunning, T. H., Jr. *J. Chem. Phys.* **1989**, *90*, 1007.
(42) Boys, S. F.; Bernardi, F. *Mol. Phys.* **1970**, *19*, 553.
(43) Valiron, P.; Mayer, I. *Chem. Phys. Lett.* **1997**, *275*, 46.
(44) Morse, P. M. *Phys. Rev.* **1929**, *34*, 57.
(45) Rajamäki, T.; Noga, J.; Valiron, P.; Halonen, L. *Mol. Phys.* **2004**, *102*, 2259.
(46) Rajamäki, T.; Kállay, M.; Noga, J.; Valiron, P.; Halonen, L. *Mol. Phys.* **2004**, *102*, 2297.
(47) Wilson, E. B.; Decius, J. C.; Cross, P. C. *Molecular Vibrations*; Dover: New York, 1980.
(48) Atkins, P. V. *Molecular Quantum Mechanics*, 2nd ed.; Oxford University Press: Oxford, 1983.
(49) Kobayashi, R.; Koch, H.; Jørgensen, P.; Lee, T. J. *Chem. Phys. Lett.* **1993**, *211*, 94.
(50) Lane, J. R.; Kjaergaard, H. G.; Plath, K. L.; Vaida, V. *J. Phys. Chem. A* **2007**, *111*, 5434.
(51) Kjaergaard, H. G.; Low, G. R.; Robinson, T. W.; Howard, D. L. *J. Phys. Chem. A* **2002**, *106*, 8955.
(52) Eckart, C. *Phys. Rev.* **1935**, *47*, 552.
(53) Le Sueur, C. R.; Miller, S.; Tennyson, J.; Sutcliffe, B. T. *Mol. Phys.* **1992**, *76*, 1147.
(54) Lawton, R. T.; Child, M. S. *Mol. Phys.* **1980**, *40*, 773.
(55) Herzberg, G. *Molecular Spectra and Molecular Structure II*, 1st ed.; Van Nostrand Reinhold Co.: New York, 1945.
(56) Child, M. S.; Halonen, L. *Adv. Chem. Phys.* **1984**, *57*, 1.
(57) Halonen, L. *Adv. Chem. Phys.* **1998**, *104*, 41.

JP903088A